

An Efficient Real-Time Vehicle Monitoring Method

Zhoujing Ye^{ID}, Member, IEEE, Ya Wei, Weidong Zhang, and Linbing Wang

Abstract—As the major transportation infrastructure, roads play an important role in intelligent transportation system. However, the intelligent level of roads is insufficient currently, which does not match the development needs of autonomous vehicles in the near future. In order to improve the intelligence level of road infrastructures, a distributed acceleration sensing node array was embedded in the pavement to collect pavement vibration signals under the action of vehicle moving load to sense the traffic information. A complete set of processing algorithms, including raw data preprocessing algorithm, same vehicle judgment algorithm and vehicle information analysis algorithm, is proposed to extract the traffic information from the monitored vibration data. The traffic information such as vehicle speed, axle numbers, wheelbases, load position, and traffic flows are obtained. The acquired traffic information can support intelligent traffic control as well as scientific road maintenance.

Index Terms—Vehicle monitoring, pavement vibration, distributed multi-nodes, pretreatment, artificial neural network.

I. INTRODUCTION

As an important enabler for driving, roads play an important role in intelligent transportation system. They should be able to sense the service status and effectively interact with automatic driving vehicles in the future. However, the intelligent level of roads is insufficient currently, which does not match the development needs of autonomous vehicles. In the field of road engineering, pavement dynamic response monitoring is one of the effective ways to improve the intelligent level of roads.

The dynamic response signal should contain the information such as dynamic load of vehicles, internal stress state of pavement and mechanical characteristics of structures due to the road-vehicle interaction [1], [2]. By analyzing the signals of pavement dynamic response, the vehicle information and the road service status can be obtained. Common monitoring sensors include stress-strain sensors [3], fiber bragg grating sensors [4], distributed optical fiber sensors [5], [6], acceleration sensors [7].

Traditionally, resistive stress-strain sensors, displacement sensors, and piezoelectric accelerometers were embedded in

Manuscript received 1 October 2021; revised 3 January 2022 and 22 January 2022; accepted 2 February 2022. Date of publication 17 March 2022; date of current version 7 November 2022. This work was supported in part by the National Key Research and Development Plan under Grant 2021YFB3202901, in part by the Beijing Major Science and Technology Projects under Grant Z191100008019002, and in part by the Technology Innovation and Demonstration Project (2021) of the Department of Transport of Yunnan Province. The Associate Editor for this article was X. Luo. (*Corresponding author: Linbing Wang*)

Zhoujing Ye and Weidong Zhang are with the National Center for Materials Service Safety, University of Science and Technology Beijing, Beijing 100083, China (e-mail: yezhoujing@ustb.edu.cn; zwd@ustb.edu.cn).

Ya Wei is with the Department of Civil Engineering, Tsinghua University, Beijing 100084, China (e-mail: yawei@mail.tsinghua.edu.cn).

Linbing Wang is with the College of Engineering, Virginia Tech, Blacksburg, VA 24061 USA (e-mail: wangl@vt.edu).

Digital Object Identifier 10.1109/TITS.2022.3150224

the pavement to monitor the pavement dynamic response. However, these sensors are large in size and less endurance [8]. Under the coupling effect of vehicle load and environmental factors, the service life of these sensors was often only a few months, which cannot meet the needs of long-term pavement performance monitoring. In addition, these sensors can neither process data nor communicate Normally, the aid from a data acquisition system is required, leading to a higher monitoring cost and large energy consumption. Consequently, it is hardly a viable option for long-term monitoring and large-scale deployment.

The advances in the Micro Electro Mechanical Systems (MEMS) technology enables sensors with greater sensitivity, higher frequency response, smaller physical size, and less power consumption for MEMS accelerometer. It embraces technical advantages such as low cost and low power consumption, high integration, miniaturization and scalability, and the ability for real-time acquisition, processing and communication, which will benefit data-driven pavement vibration response monitoring [9].

In some studies of pavement vibration monitoring, MEMS acceleration sensors are deployed at the roadside for vehicle speed monitoring, vehicle classification and traffic counting [10]–[14]. Restrained by the resolution of existing acceleration sensors and the exponential attenuation characteristics of road vibration, roadside deployment cannot provide useful and efficient signals of the dynamic response from pavement. Some studies propose to combine acceleration sensor array and geomagnetic sensor to collect the information of speed, type, and weight of vehicles. The wireless sensor network (WSN) is developed, the geomagnetic sensor is used to monitor the arrival and departure time of vehicles, while an acceleration sensor is applied to detect axles [15]–[17]. However, the WSN network suffers from packet loss and energy limitation, and the time synchronization of different types of sensors makes the system data processing algorithm more complicated. Once the geomagnetic sensor fails, the whole system tends to break down.

In view of the above situations, this study proposes a set of data processing algorithms for analyzing the traffic information from the vibration data collected from the embedded sensor nodes. The algorithms are then verified by extracting the traffic information of a real road with vibration sensor nodes embedded. The method introduced in this study can be used for the long-term traffic and service status monitoring of pavements.

II. SENSOR DEPLOYMENT

The developed acceleration sensing node is used to realize real-time monitoring of the pavement vibration under the vehicle moving load. The acceleration sensing node is encapsulated

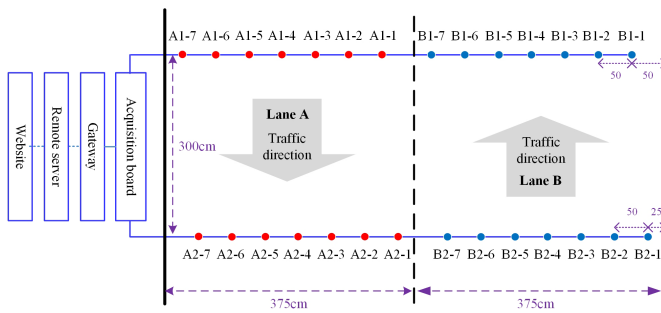


Fig. 1. Schematic diagram of acceleration sensing node deployment.

TABLE I
STRUCTURE OF TEST SECTION

Layer	Materials	Thickness (cm)	Density (kg/m ³)	Modulus (Mpa)	Poisson's ratio
Surface layer	AC-13	15	2300	1200	0.35
Base layer	Gravel	24	2200	900	0.35
Subgrade	Soil	—	1800	50	0.4

sulated in casting nylon, which can withstand repeated vehicle loads. The silicone rubber is filled to cover the Printed Circuit Board (PCB), which can prevent the water from infiltrating into the package box and causing any damage to the PCB under the hydrodynamic pressure of pavement. The multiple acceleration sensing nodes were deployed on 320 National Highway in Kunming, Yunnan Province. The deployment of sensing nodes is shown in Fig. 1.

The monitored road section has two lanes (lane A and lane B), each with a width of 375cm and equipped with two layers of acceleration sensing nodes with an interval of 300cm. There are seven acceleration sensing nodes in each layer. The adjacent nodes in the same layer have an interval of 50cm. The two layers of nodes in each lane are arranged with a dislocation of 25cm to capture the axle loading area as much as possible. Each node is numbered according to the locations of lanes and layers. A1-7 represents the No.7 acceleration sensing node in the first layer of Lane A, and B2-3 represents the No.3 acceleration sensing node in the second layer of Lane B.

The embedding depth of all the sensing nodes is 3cm, the distance between the top surface of the sensing node and the road surface. The type and thickness of the test section are obtained through core sampling, as shown in Table I.

The acceleration sensing nodes collect pavement vibration signals at a sampling frequency of 500 Hz. The collected voltage signal that can reflect the vibration is converted into a long-distance transmission and anti-noise current signal, which is transmitted to the acquisition board through the cable. Then the current signal output via multiple nodes on the acquisition board is converted into the voltage signal, and further converted into a digital signal to be transmitted to the gateway through the network cable. The gateway realizes the communication between the sensor network and the remote server. After further processing, the data in the remote server

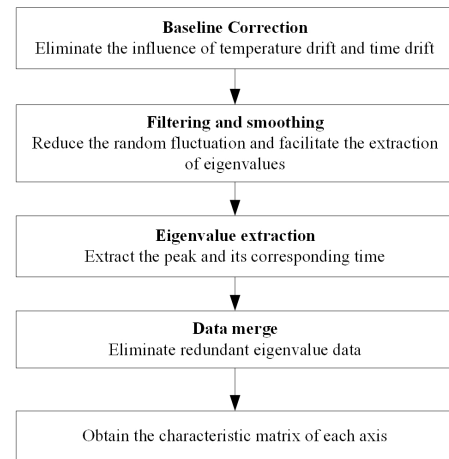


Fig. 2. The raw data preprocessing algorithm.

can be visualized on the web page. The processing algorithms will be discussed below. This system is powered by a 12 V battery and solar energy [18].

III. RAW DATA PREPROCESSING

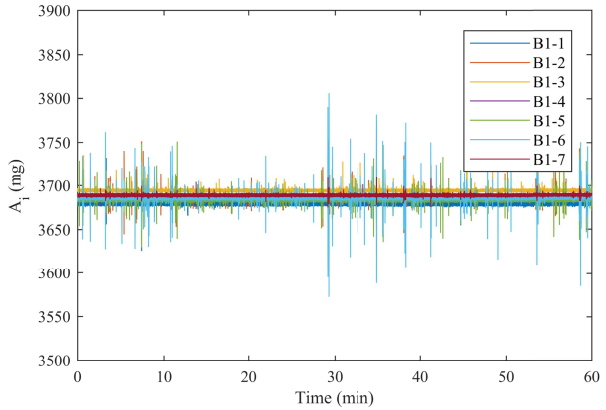
The amount of pavement vibration data collected by 28 acceleration sensing nodes in real-time is large, and the baseline of the raw data collected by each node is different. In order to improve the computational efficiency and to reduce data redundancy, communication cost, and system energy-consuming, it is necessary to preprocess the raw data first. The flow of the raw data preprocessing algorithm is shown in Fig. 2.

The original data of each node should be first calibrated by baseline correction to eliminate the influence of temperature drift and time drift. The calibrated data is then filtered and smoothed to reduce the random fluctuations and facilitate feature extraction. And then, the eigenvalue data of peak and the corresponding time are extracted from the smoothed data of each node. Due to the spatial distribution of nodes and the time information of signals, the formed eigenvalue matrix contains spatio-temporal information. Finally, the eigenvalue data in the matrix are merged to eliminate redundant data produced by the multi-nodes. Through the above raw data preprocessing algorithm, the characteristic matrix of an acceleration sensor array under the action of each axle is obtained, which provides data for the same vehicle judgment algorithm.

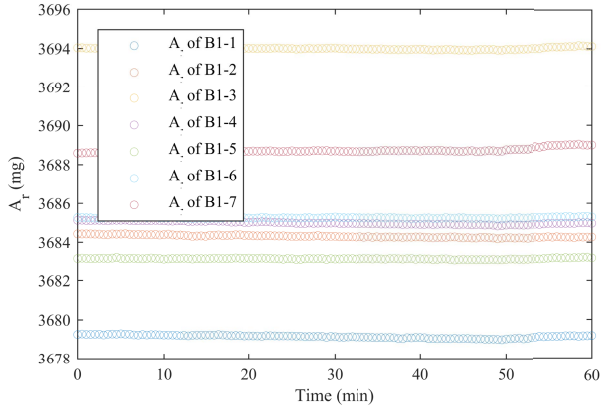
A. Baseline Correction

Fig. 3 (a) shows the raw vibration data monitored by B1 sensing nodes within one hour. The baseline of each node is different due to the thermal deformation of the sensing material and the random errors in the circuit. The output signal of the acceleration sensing node has zero drift phenomenon. It is necessary to correct baseline of the raw data collected by each node.

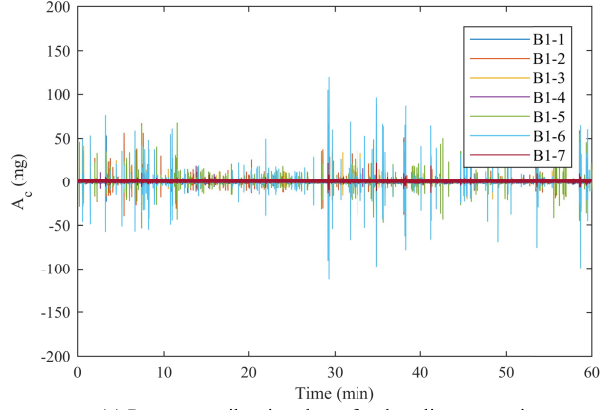
Each node sends the raw data to the gateway, and the gateway uploads the raw data every 30s to the cloud platform



(a) Zero drift phenomenon of acceleration sensing nodes



(b) Reference value of signal data within every 30s of 120 segments



(c) Pavement vibration data after baseline correction

Fig. 3. Baseline correction of raw data of pavement vibration.

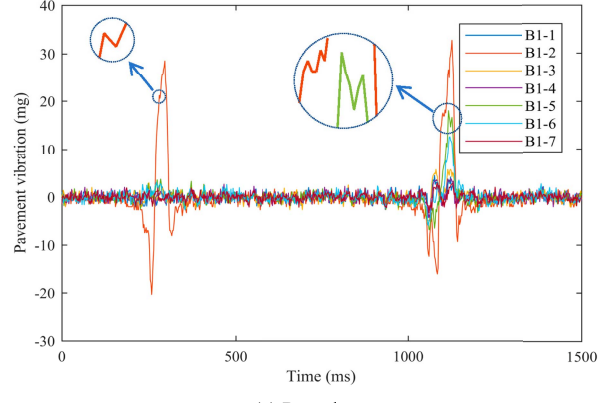
as a data packet. The reference value of raw data within the 30s is calculated by the least square method, that is, the sum of squares of errors between the reference value to be determined and the monitored data should be the smallest. The reference value (A_r) is calculated by using the linear regression method in MATLAB. The calculation formula is as follows:

$$A_r = \text{regress}(y, X) \quad (1)$$

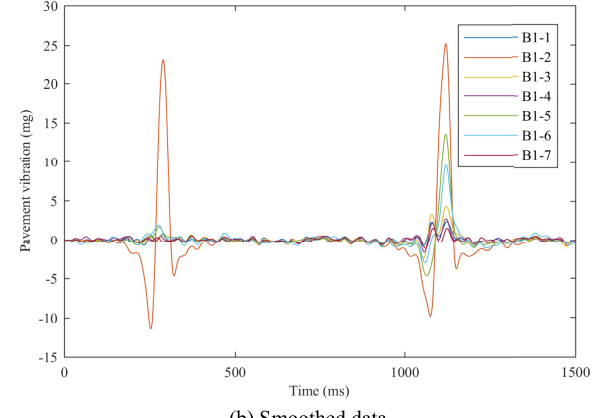
$$y = [A_1; A_2; A_3; \dots; A_i] \quad i = 15000$$

$$x = [1; 1; 1; \dots; 1] \quad \text{length}(X) = 15000$$

$$A_c = A_i - A_r \quad (2)$$



(a) Raw data



(b) Smoothed data

Fig. 4. Vibration data of B1 monitoring points.

where A_r is the reference value of raw data within the 30s, i.e. regression value for raw data within 30s. A_i is the monitored value of each point. There are 15000 points in y because the sampling rate is 500Hz and the time is the 30s. X is a vector composed of one, and its length is consistent with y , a total of 15000. A_c is the vibration data after baseline correction.

There are 120 segments in one hour because of the 30s as a segment. Therefore, 120 values of A_r are calculated, as shown in Fig. 3(b). Then the corresponding A_r value is subtracted from the original data A_i in every 30s to obtain the correct vibration data, as shown in Fig. 3(c). Through baseline correction, the original data collected by these nodes have the same baseline value, i.e. zero. At this time, it is convenient to compare the vibration amplitude generated by each node.

B. Filtering and Smoothing

When the vehicle passes through the monitored area, the road vibration signal will generate peaks corresponding to the axle. Fig. 4(a) shows the original road vibration signal when a two-axle vehicle passes through B1 nodes, and the number of peaks corresponds to the number of axles.

Under the influence of vehicle vibration and environmental noise, the original vibration data have multiple maxima at the peak, and the time points corresponding to the vibration peaks are not unique (Fig. 4a), which leads to inaccurate speed and shaft length calculated by the time difference. In order to

Time difference (ms)	Absolute time (ms)	B1-1 (mg)	B1-2 (mg)	B1-3 (mg)	B1-4 (mg)	B1-5 (mg)	B1-6 (mg)	B1-7 (mg)
0	9129684	0	10.5	0	0	0	0	0
2	9129686	16.2	0	0	0	0	0	0
0	9129686	0	0	6.7	0	0	0	0
4	9129690	0	0	0	0	13.3	0	0
4	9129694	0	0	0	0	0	20.3	0
240	9129934	10.6	0	0	0	0	0	0
0	9129934	0	7.6	0	0	0	0	0
12	9129946	0	0	0	0	11.3	0	0
2	9129948	0	0	0	0	0	10.2	0
9860	9139808	0	0	8.1	0	0	0	0
2528	9142336	0	0	10.5	0	0	0	0
474	9142810	0	0	13.3	0	0	0	0
1840	9144650	0	0	8.5	0	0	0	0
4	9144654	0	0	0	0	0	9.4	0
442	9145096	0	0	7.9	0	0	0	0
5014	9150110	0	9.1	0	0	0	0	0
2	9150112	0	0	0	0	10.3	0	0
560	9150672	4.8	0	0	0	0	0	0
2	9150674	0	0	0	0	0	7.8	0
6	9150680	0	22.5	0	0	0	0	0
2	9150682	0	0	0	0	40.3	0	0
...

Data merge								
Time difference (ms)	Absolute time (ms)	B1-1 (mg)	B1-2 (mg)	B1-3 (mg)	B1-4 (mg)	B1-5 (mg)	B1-6 (mg)	B1-7 (mg)
0	9129694	16.2	10.5	6.7	0	13.3	20.3	0
252	9129946	10.6	7.6	0	0	11.3	10.2	0
9862	9139808	0	0	8.1	0	0	0	0
2528	9142336	0	0	10.5	0	0	0	0
474	9142810	0	0	13.3	0	0	0	0
1844	9144654	0	0	8.5	0	0	9.4	0
442	9145096	0	0	7.9	0	0	0	0
5016	9150112	0	9.1	0	0	10.3	0	0
570	9150682	4.8	22.5	0	0	40.3	7.8	0
...

Fig. 5. Feature matrix of sensing nodes in B1.

obtain the unique vibration peak and the corresponding time point, Gaussian filter is used to smooth the original data [19]. Fig. 4(b) shows the smoothed data, and thus it is now easier to identify peaks and the corresponding time points.

C. Eigenvalue Extraction

The maxima of vibration signal of each node and the corresponding time can be obtained from the above smoothed data. According to the spatial deployment of each node in the layer, a feature matrix is formed, as shown in Fig. 5.

The first column represents the time difference, that is, the time difference between two adjacent rows of absolute times. The second column shows the absolute time corresponding to the peak vibration amplitude value of the node. The columns from the third to the ninth correspond to the node numbers, which store the peak values of the corresponding node numbers. Similarly, node data in column B2 is also stored in this form.

D. Data Merge

In the actual monitoring, when the vehicle passes through the monitored area, the left and right wheels on the same axle are not always perpendicular to the same line of nodes, thus leading to time difference between the peaks of the same line of nodes under the action of the same axle. Therefore, the rows with time difference less than 50ms in Fig. 5 are merged into one row, and the time corresponding to the node with the largest amplitude is selected and treated as the excitation from

one axle. Thus, each row after data merge in Fig. 5 corresponds to one axle.

In the 45 minutes monitoring video, the number of axles in the two lanes is 5312. Based on the above algorithm, the number of detected axles is 5260, and the number of undetected axles is only 52. The accuracy of axle counting is 99.2%. The reasons for the missing axle are low speed (passing at low speed), light vehicle (such as tricycle and mini-vehicle), as well as data loss from sensing nodes in the process of data collection, transmission and time synchronization.

IV. SAME VEHICLE JUDGMENT

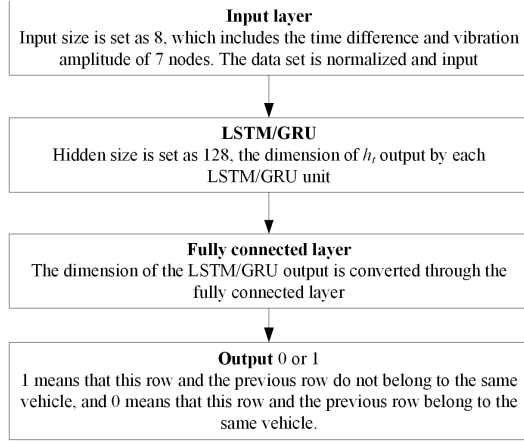
A. Related Work

Traditional axle inspection methods include tape switches, pneumatic tubes and piezoceramic sensors. These methods are easy to install and the accuracy meets the application requirements. But they have high cost and low durability (usually two years). Moreover, they may interfere with traffic during installation and replacement [20]–[22]. With the goal of freeing the use of axle detectors on the road surface, the Weighing-in-Motion of Axles and Vehicles for Europe (WAVE) project puts forward the concepts of nothing-on-road (NOR) systems and the free-of-axle detector (FAD) algorithms. Axles are usually monitored by adding additional dynamic response sensors or roadside equipment, such as shear strains, fiber optical sensors, and inductive loop detectors [23]–[26]. However, this technique is susceptible to errors in the original data. It is difficult to obtain axle information from the strain signal, because not every axle passes through with a wave crest [20]–[21]. For axle detection based on inductive loop detectors, its accuracy cannot meet the requirements of more detailed classification [22].

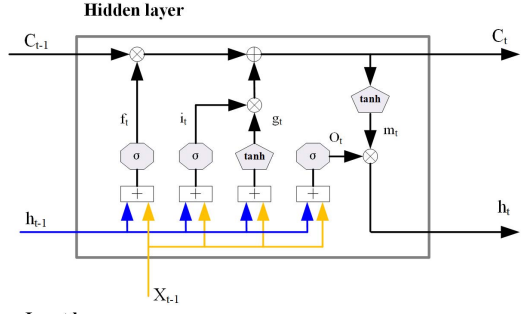
In addition, the infrared vehicle separators, radar and video imaging system placed on the roadside are used for the same vehicle judgment. But they are vulnerable to weather, traffic obstruction and need to work with other types of sensors, such as quartz piezoelectric sensors and acceleration sensors to form the weight-in-motion system [15]. Although using different types of sensors can complement each other to conduct the same vehicle judgment, this method leads to the complexity of the system. Moreover, the monitoring system consists of different sensors, such as geomagnetic sensor combined with acceleration sensor, quartz piezoelectric sensor combined with inductive loop detector. The inductive loop detector or geomagnetic sensor is used to monitor the arrival and departure time of vehicles, so as to judge the same vehicle. However, This kind of system needs to process different types of data formats; the time synchronization of different types of sensors is required; Once a certain type of sensor fails, the entire system will not operate effectively. The advantage of the method proposed in this paper is to realize same vehicle judgment by one kind of sensor, i.e., embedding only two layers of acceleration sensing nodes, without using geomagnetic sensor.

B. Model Establish

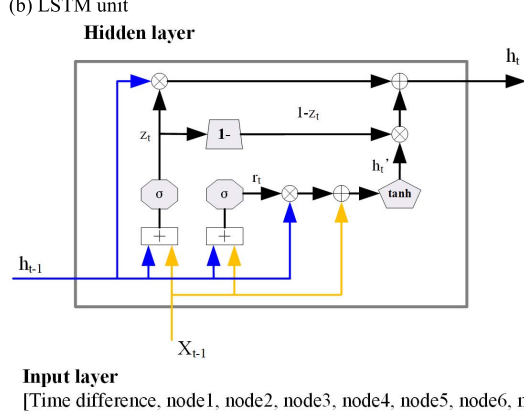
Through the above preprocessing algorithm, each row in the feature matrix corresponds to one axle, but it is not clear



(a) Macroarchitectural view of the same vehicle judgment model



(b) LSTM unit



(c) GRU unit

Fig. 6. Same vehicle judgment model.

which axles belong to the same vehicle. Therefore, in order to effectively distinguish which axle belongs to the same vehicle, the same vehicle judgment method is proposed.

The feature matrix of each layer nodes is the basic data for the same vehicle judgment. In this study, LSTM (Long Short-Term Memory) [27], [28] and GRU (Gated Recurrent Unit) [29] are used to process this data. The same vehicle judgment model is composed of the input layer, the LSTM layer /GRU layer, the fully connected layer and the output layer, as shown in Fig. 6.

C. Model Training

1) **Data Set:** The feature matrix of each layer nodes corresponds to the behavior of axles in lanes A and B, taking lane A as an example, the input data set format is shown in Fig 7.

Sensing node location	Time (ms)	1 (mg)	2 (mg)	3 (mg)	4 (mg)	5 (mg)	6 (mg)	7 (mg)	Label
A2	234	0	0	0	0	0	0	29.76	0
A2	9616	0	0	10.0	0	0	14.3	0	1
A2	242	0	0	12.7	0	0	8.7	0	0
A1	12654	0	0	0	4.8	0	0	0	1
A2	7174	0	0	0	0	0	15.6	0	1
A2	236	0	0	0	0	0	27.9	0	0
A1	7020	0	143.5	0	0	0	37.1	0	0
A2	278	12.9	0	0	0	0	0	0	0
A1	34	0	65.7	0	0	0	12.9	0	0
A2	286	9.7	0	0	18.0	0	0	0	0

Fig. 7. The data set of A lane.

TABLE II
CONFUSION MATRIX

		Actual results	
		1	0
Predicted results	1	TP	FP
	0	FN	TN

The data set includes sensing node location, the time difference between adjacent rows, the vibration amplitude of each sensing node, and the corresponding label. The value of label is 1 or 0, 1 means that this row and the previous row do not belong to the same vehicle, and 0 means that this row and the previous row belong to the same vehicle. The value of label was validated by the video. These data set will be used to train, validate, and test the proposed method for same vehicle judgement.

2) **Data Set Normalization:** Before model training, the vibration amplitude of each sensing node needs to be normalized. Normalization can speed up the gradient descent to find the optimal solution and help to improve the accuracy of the model. After normalization, the vibration amplitude range of each node is $[0,1]$, and the mathematical formula for normalization is as follows:

$$\tilde{x}_i = \frac{x_i - \min}{\max - \min} \quad (3)$$

where, max is the maximum value of vibration amplitude in the data set, and min is the minimum value of vibration amplitude in the data set.

3) **Evaluation Index:** In order to evaluate the performance of LSTM/GRU-based same vehicle judgment model, six evaluation indexes, including confusion matrix, accuracy, precision, recall rate, F1-score and training time, are used to evaluate the performance of the model.

As the same vehicle judgment model is a binary classification model, if the predicted results are combined with the actual results, the following four situations will occur, forming a confusion matrix, as shown in Table II.

Accuracy is defined as the percentage of the predicted correct results in the total samples, and its formula is as follows:

$$\text{Accuracy} = \frac{TP + TN}{TP + TN + FP + FN} \quad (4)$$

TABLE III
THE HARDWARE AND SOFTWARE CONFIGURATION

Item	Configuration
CPU	AMD Ryzen 7 3700X 8-Core Processor
Internal storage	16G
Operating system	Windows
Programing language	Python 3.8.0
Deep learning framework	PyTorch

P (positive) stands for 1; N (negative) stands for 0; T (true) means the prediction is correct; F (false) means the prediction is error. TP means the predicted result is 1 and actual result is 1; FP means the predicted result is 1 but actual result is 0; FN means the predicted result is 0 but actual result is 1; TN means the predicted result is 0 and actual result is 0.

Precision is defined as the prediction accuracy in the positive sample results, and its formula is as follows:

$$\text{Precision} = \frac{TP}{TP + FP} \quad (5)$$

Recall rate is the probability of being predicted as a positive sample among the actually positive samples, and its formula is as follows:

$$\text{Recall} = \frac{TP}{TP + FN} \quad (6)$$

F1-score is used to comprehensively evaluate the performance of precision and recall. The larger the F1-score, the higher the quality of the model.

$$\text{F1-score} = \frac{2 \times \text{Precision} \times \text{Recall}}{\text{Precision} + \text{Recall}} \quad (7)$$

Training time is defined as the processing time of all learning epoch of the training set under the same configuration.

4) Configuration Environment: The hardware and software configuration for the model training is shown in Table III. The hardware of the model mainly depends on CPU, and the software is PyTorch deep learning framework.

5) Model Parameters: The input size is set as 8, including the time difference and vibration amplitude of 7 nodes. Hidden size is set as 128, that is, the dimension of h_t output by each LSTM unit. h_t is the state of the hidden layer at time t . Num layer is set as 2, which indicates the number of LSTM units. Batch size is set as 256 indicating how many groups of data set are input each time, which affects the model's generalization performance. Time step is set as 31, which means that each group inputs 31 rows of data. Learning rate is set as 0.0003. The learning rate affects the convergence state of the model. When the learning rate is set too small, the convergence process will become very slow. When the learning rate is set too large, the gradient may oscillate back and forth near the minimum value, and may even fail to converge. Epochs is set as 2000, which indicates the times of iteration. Although the increase of iteration rounds can reduce the training error, it will also increase training time. Test size is set as 0.2, which means that the ratio of training dataset to validation dataset is 8:2.

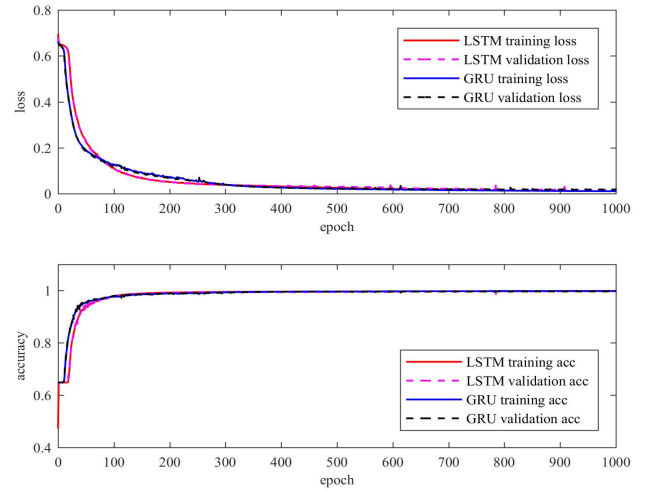


Fig. 8. Accuracy and loss value of LSTM and GRU in training process.

TABLE IV
SINGLE-VEHICLE RECOGNITION PERFORMANCE OF LSTM/GRU

Parameters	LSTM	GRU
Accuracy	99.78%	99.72%
Precision	99.60%	99.57%
Recall	99.77%	99.62%
F1-score	0.997	0.996
Training duration	5648.6s	4851.5s

D. Result Analysis

In the training process, the value of accuracy and loss of the training dataset and validation dataset are shown in Fig. 8. The changing trend of the accuracy and the loss value can be used to judge whether the model converges or overfits.

In Fig. 8, when the epoch is from 0 to 200, the accuracy of the train set and validation set increases rapidly, while the loss value decreases, indicating that the network is still learning. In the range of 200-1000 epoch times, the accuracy rate of the training dataset increases slowly, while the loss value decreases slowly, which indicates that the network model is constantly learning and there is no "over-fitting" phenomenon. After model training, the confusion matrix of the validation set is output, and the accuracy, precision, recall, F1-score and training duration of the model are calculated, as shown in Table IV.

The trained model has high accuracy for same vehicle judgment, up to 99.5%. The error mainly comes from low vehicle speed (<10km/h) and record error when labeling manually. Although LSTM has a slightly higher accuracy than GRU. GRU has notable advantages in training time, with nearly 797.1s saved, or, 13 minutes. As the training data increase, GRU will have greater efficiency.

V. VEHICLE INFORMATION ANALYSIS

After done with the same vehicle judgment, the time when each axle of the vehicle passes through the monitoring area can be obtained. According to the time when the first axle

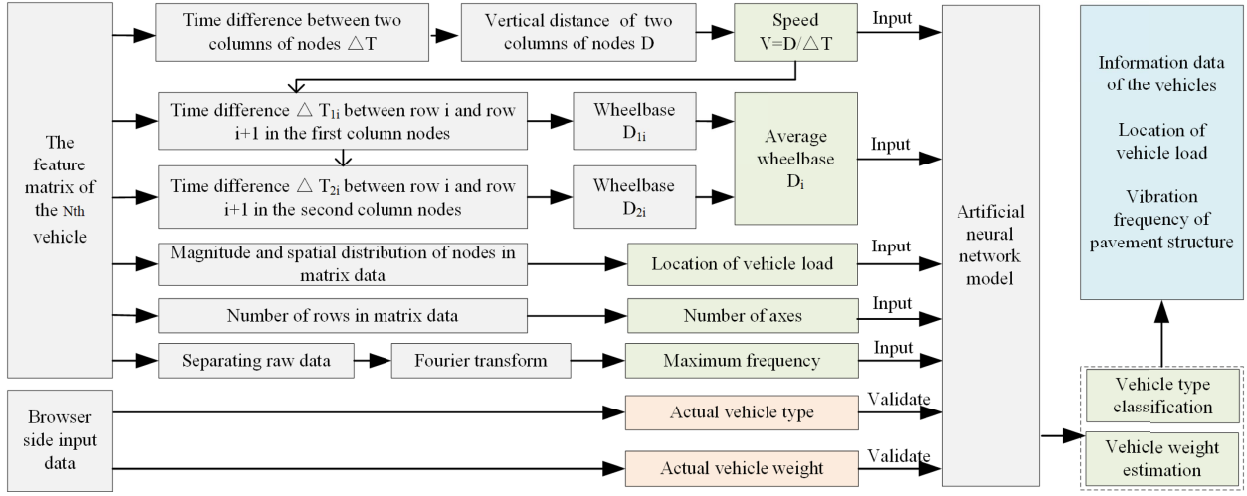


Fig. 9. Flow chart of vehicle information analysis algorithm.

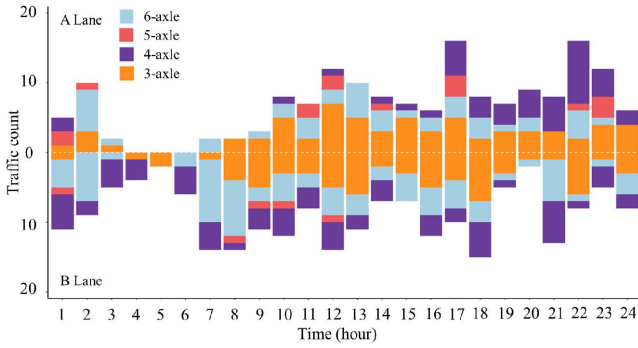


Fig. 10. Traffic count of large vehicles of the two lanes over 24 hours.

of the vehicle enters the monitoring area and the last axle leaves the monitoring area, the raw vibration data corresponding to the single vehicle can be obtained. The feature matrix of the vehicle is calculated by the raw data preprocessing. Then the vehicle information can be analyzed based on the feature matrix of two layers of nodes. Fig. 9 shows the flow chart of vehicle information analysis algorithm.

A. Traffic Volume

Traffic volume information refers to the number of different types of vehicles passing through the monitoring area in a certain period of time, which is calculated as follows:

$$SS = \sum S_i \quad (8)$$

where i indicates the type of vehicles, S_i is the number of each type of vehicles, and SS is the sum of the number of different types of vehicles. The number of rows of the feature matrix represents the number of axles of the vehicle. Fig. 10 shows the variation of three-axle, four-axle, five-axle and six-axle vehicles on the two lanes within 24 hours.

The number of three-axle vehicles is the largest, followed by four-axle and six-axle vehicles, and the number of five-axle vehicles is the least. The number of large vehicles passing the B lane is slightly greater than that of A lane. Especially, the number of large vehicles reaches the maximum

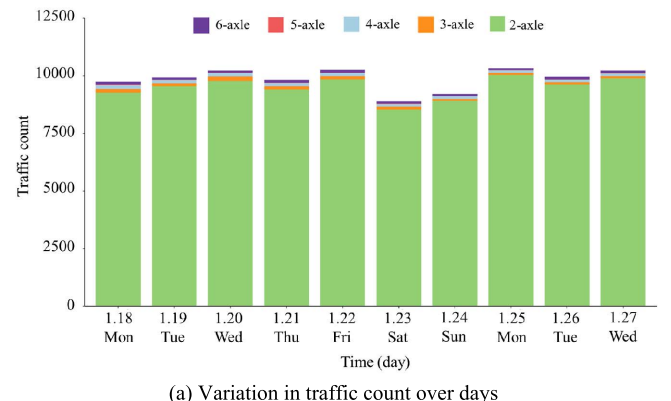


Fig. 11. Traffic statistics during a time period of 10 days.

in 11:00 -12:00, 16:00 - 17:00 and 21:00 - 22:00, and the minimum in 3:00 - 6:00.

The traffic statistics during a time period of 10 days is shown in Fig. 11. The daily traffic statistics can reflect variation in traffic count over days and the proportion of different vehicles.

In Fig. 11, the daily traffic volume is approximately 10,000 vehicles per day on weekdays, and 9,000 vehicles per day on weekends. The proportion of two-axle vehicles was 96.21%. Among vehicles with over three axles, four-axle vehicles had the maximum proportion, as high as 1.30%, followed by three-axle vehicles (1.28%), six-axle vehicles (1.03%), and five-axle vehicles (0.19%). The traffic volume and proportion can

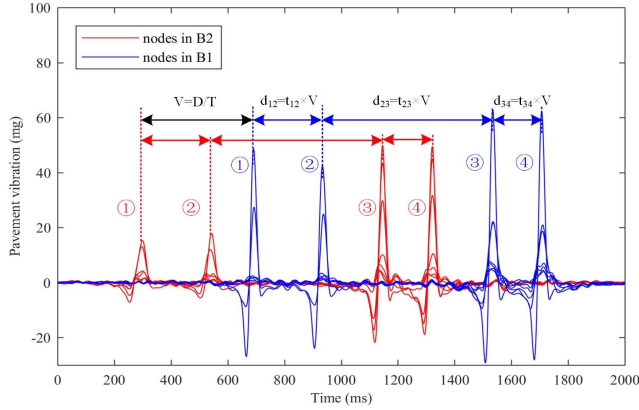


Fig. 12. Pavement vibration data of a four-axle vehicle.

show the transportation activity in the monitored section and indirectly reflect the local economy, which provides data for regional economy evaluation and road network planning.

B. Speed, Number of Axles and Wheelbase

The pavement vibration signal under vehicle moving load can be used to obtain vehicle speed, axle number and wheelbase. Fig. 12 shows the pavement vibration signal of a 4-axle vehicle passing through the monitoring area.

The first two peaks of nodes in B2 are obviously lower than those of nodes in B1. Because the first two axles of the vehicle have a single tire on each side and the nodes in B1 and B2 are arranged with a dislocation of 25cm, when the vehicle passes B2, the first two axles do not press the sensing nodes, but press the sensing nodes in B1. As a result, the amplitude of B1 corresponding to the front axle is larger than that of B2. There is no much difference in peak amplitude between the two rear axles. Because the two rear axles of the vehicle are two tires on each side, the loading area is wide, and the sensing nodes in each layer can both be pressed. The vehicle speed can be calculated as follows:

$$V = \frac{D_{12}}{T_{1i} - T_{2j}} \quad (9)$$

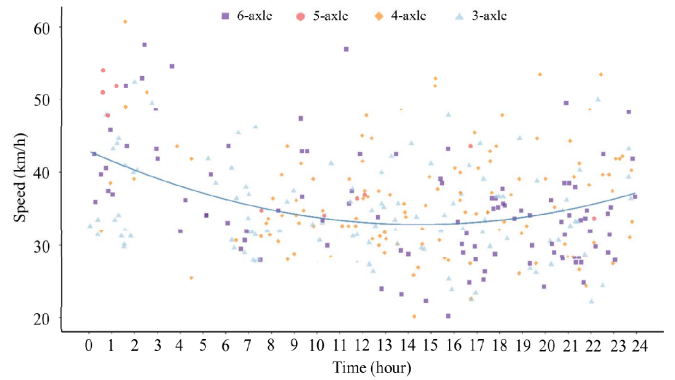
where D_{12} is the vertical distance (along the driving direction) between nodes in the first layer and the second layer. T_{1i} and T_{2j} are the time corresponding to node i in the first layer and node j in the second layer respectively. i is the number of the node generating the maximum amplitude in the first layer under the action of vehicle front axle, and j is the number of nodes generating the maximum amplitude in the second layer.

Given the vehicle speed, the wheelbase of adjacent axles is calculated according to the vehicle speed and the time difference of each peak in the same layer. According to the data of nodes in B1 and B2, the average wheelbase can be obtained, and the calculation formula is as follows:

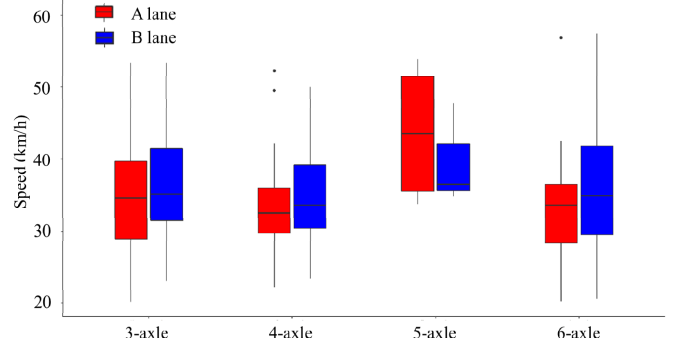
$$A_i = V \times (T_{ir} - T_{if}) \quad (10)$$

$$\bar{A} = \frac{\sum_{i=1}^n A_i}{n} \quad (11)$$

where A_i is the wheelbase between the front axle and the rear axle calculated according to the node signal of the i th



(a) Speed distribution over time for different types of vehicles



(b) Speed statistics of different types of vehicles in different lanes

Fig. 13. The speed distribution of large vehicles in a day.

layer. T_{ir} is the time corresponding to the maximum amplitude of the rear axle in the node of the i th layer. T_{if} is the time corresponding to the maximum amplitude of the front axle in the node of the i th layer. \bar{A} is the average wheelbase of the front axle and the rear axle. n is the layer number of embedded nodes, which is set to 2.

According to the above calculation, the vehicle speed is 27.55 km/h, the wheelbase in Fig. 10 is $d_{12} = 1.85$ m, $d_{23} = 4.62$ m and $d_{34} = 1.35$ m. The number of axles is the calculated wheelbase plus one, that is, 4. The accuracy of vehicle speed and wheelbase monitoring based on pavement vibration has been verified. Through the video, the brand and model of vehicles are obtained, the actual wheelbase was acquired from the specifications from the vehicle manufacturer. Since the wheelbase was calculated based on the calculated speed. The result also indirectly verifies that the calculated speed was accurate. After verification, the monitoring accuracy of wheelbase can reach above 96%. But this system is not suitable for vehicle information monitoring in congested traffic. The low vehicle speed (<5km/h) will result in a small road vibration amplitude. The smaller vibration amplitude will make the sensing node more susceptible to noise and the environment [19], [30].

Fig. 13 shows the speed distribution of large vehicles within a day. The vehicle speed at night is faster than that at daytime. The vehicle speed at daytime is basically within the range of 20km/h-50km/h, and it is 30km/h-60km/h after 0:00. The speed of three-axle, four-axle and six-axle vehicles in B lane is slightly faster than that in A lane. The generally faster vehicle

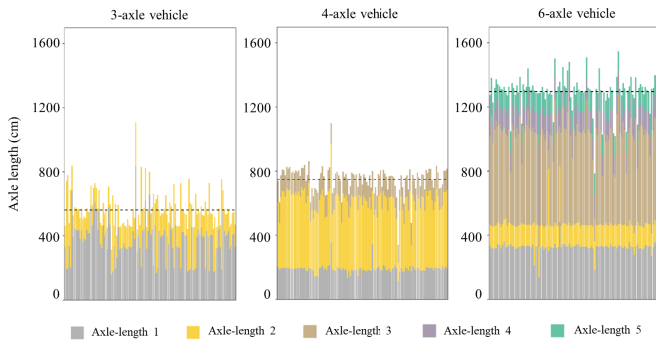


Fig. 14. The distance between axles varies from different types of vehicles.

speed of five-axle vehicles is mainly due to the small size of sample data and the night driving. By monitoring different vehicles, lanes, and vehicle speed in different time frames, the system can statistically analyze the range of the vehicle driving speed in different road sections. It can not only improve the efficiency of the traffic operation, but also realize refined traffic control by vehicle-road interaction, such as overspeed warning, precise time setting for tidal flow lane, speed limit setting for different vehicles, and the autonomous driving speed setting for self-driving cars. Through larger deployment and real-time traffic monitoring, the system is also conducive to the realization of the beyond visual range driving of vehicles.

As shown in Fig. 14, the average of total axle length of three-axle, four-axle and six-axle vehicles is 5.62m, 7.49m, and 12.97m, respectively. Even for the same type of vehicle, the distance between axles is also different. Among them, the total axle length of three-axle vehicles has the largest range of variation, followed by four-axle vehicles and six-axle vehicles. The classification for vehicle type can be made according to the axle length of vehicles and the local classification standards.

C. Location of Vehicle Load

In the monitoring of vibration response of asphalt pavement, the nodes right under the weight have obvious peaks, while the vibration amplitude of nodes away from the position of load decreases rapidly. The position of vehicle load can be determined according to this phenomenon. There are 2 layers of acceleration sensing nodes in each lane and 7 acceleration sensing nodes in each layer, the adjacent nodes in the same layer have an interval of 50cm. The two layers of nodes are arranged with a dislocation of 25cm. Therefore, in each lane, there are 14 points corresponding to different spatial positions so as to capture the axle loading area as much as possible.

Fig. 15 shows how the amplitude of each axle corresponds to each node when a 4-axle vehicle pass through the monitoring area. The two front axles of the 4-axle vehicle act on the areas of 100-125 and 300-325, while the two rear axles act on the areas of 75-175 and 250-350. The load position of each axle of the vehicle is determined. According to the range of load acting areas, it can be judged that the two front axles of the vehicle have a single tire on each side, and the two rear axles double tires.

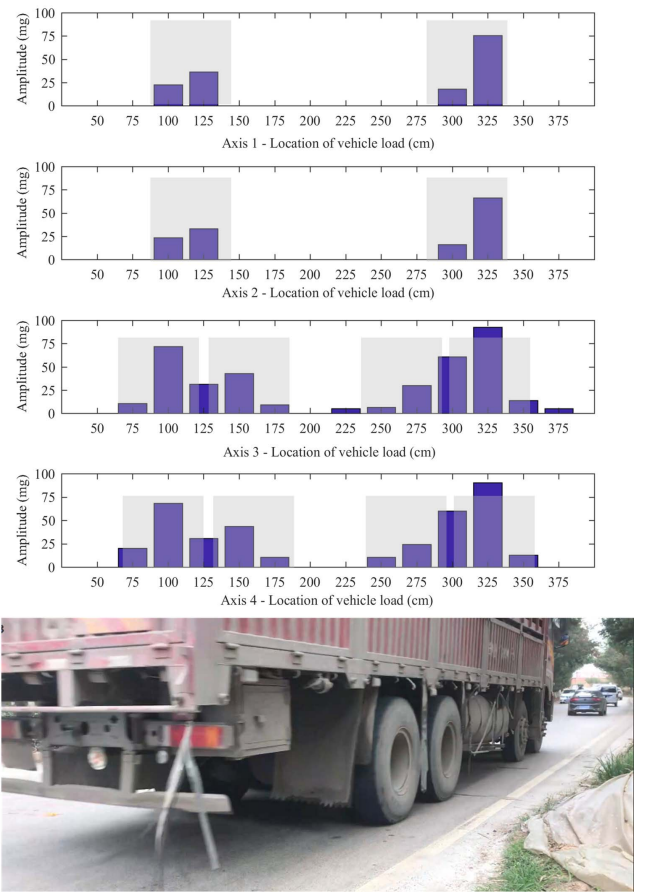


Fig. 15. Location of vehicle load.

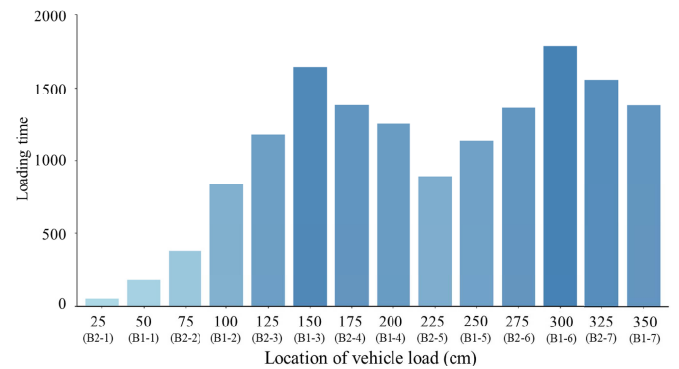


Fig. 16. Loading times of large vehicles on B lane within a week.

The loading times of large vehicles (above 3-axle) on B lane within a week is shown in Fig. 16. The main location of vehicle load in the monitoring area can be determined through the accumulated loading times. In Fig. 16, vehicles mostly travel inside the road. The loading times of roadside location (B2-1, B1-1) is less. The road central area of B2-5 suffers less from the vehicle load, while the area near to B1-3 and B1-6 suffers more from the vehicle load and rutting and crack occur there. The location of vehicle load can help judge axle load, axle type, and axle count. The information of vehicle, road structure, material, and temperature are critical for estimating

the service condition of the road, which can be used for predicting road diseases, such as rutting and cracking. It is helpful to carry out timely road maintenance by monitoring the location of vehicle load and the accumulated loading times.

VI. SUMMARY AND PROSPECT

Traditional pavement monitoring sensors, such as stress-strain sensors, fiber optical sensors, displacement sensors and piezoelectric accelerometers, can neither process data nor communicate. Normally a data acquisition system is required, which leads to a higher monitoring cost as well as large energy consumption. The acceleration sensing node based on the MEMS technology can integrate low-cost and low-power electronic components through the circuit design of PCB, which realizes data acquisition, filtering, processing, and transmission at the sensing terminal and really benefits data-driven pavement vibration response monitoring. This paper developed a multi-node sensing array to obtain the multi-point vibration data of the pavement under the moving load of vehicles. A complete set of pavement vibration data processing algorithm is proposed. The multi-node sensing array and the algorithms were then validated by field implementation, and the useful traffic information were obtained. The major conclusions are drawn as follows:

A data preprocessing algorithm is proposed to extract the feature data from pavement vibration behavior monitored from a set of multi-node sensing array. There are four steps: baseline correction, filtering and smoothing, eigenvalue extraction and data merge. The feature matrix is formed after preprocessing, which contains the amplitudes of each node and its corresponding time. Each row in the feature matrix corresponds to one axle. Then a same vehicle judgment model based on LSTM/GRU was established based on the feature matrix data. The same vehicle judgement with high-precision (99.5%) is achieved by embedding only two layers of acceleration sensing nodes, without equipping geomagnetic sensor or infrared sensor. This method has all-weather same vehicle judgment ability due to the embedded monitoring. Finally, a vehicle information analysis algorithm was proposed. The information such as vehicle speed, axle length (axle type, vehicle type), load position, traffic flow was analyzed according to the pavement vibration data of single-vehicle.

The pavement vibration analysis method proposed in this study is one of the core technologies of smart road, which improves the intelligence level of roads. The acquired traffic information provides necessary data for intelligent traffic control and scientific road maintenance. In the future, the system's durability should be evaluated and improved by optimizing packaging and construction methods of sensing nodes to achieve long-term monitoring.

ACKNOWLEDGMENT

The authors would like to thank the Research Institute of Highway Science and Technology for the support of the asphalt pavement vibration monitoring.

REFERENCES

- [1] Z. H. Dong and P. M. Lv, "A model to study the dynamic response of visco-elastic layered system under moving load," *Eng. Mech.*, vol. 28, no. 12, pp. 153–159, 2011.
- [2] H. Wang, I. L. Al-Qadi, and I. Stanciuescu, "Effect of surface friction on tire-pavement contact stresses during vehicle maneuvering," *J. Eng. Mech.*, vol. 140, no. 4, Apr. 2014, Art. no. 04014001.
- [3] W. Xue, D. Wang, and L. Wang, "Monitoring the speed, configurations, and weight of vehicles using an *in-situ* wireless sensing network," *IEEE Trans. Intell. Transp. Syst.*, vol. 16, no. 4, pp. 1667–1675, Aug. 2015.
- [4] Z. J. Dong, Y. Q. Tan, and J. P. Ou, "Dynamic response analysis of asphalt pavement under three-directional nonuniform moving load," *China civil Eng. J.*, vol. 46, no. 6, pp. 122–130, 2013.
- [5] W. Liu *et al.*, "A subgrade cracking monitoring sensor based on optical fiber sensing technique," *Structural Control Health Monitor.*, vol. 25, no. 9, Sep. 2018, Art. no. e2213.
- [6] H. Zhao *et al.*, "Support conditions assessment of concrete pavement slab using distributed optical fiber sensor," *Transportmetrica A, Transp. Sci.*, vol. 15, no. 1, pp. 71–90, 2018.
- [7] E. Levenberg, "Inferring pavement properties using an embedded accelerometer," *Int. J. Transp. Sci. Technol.*, vol. 1, no. 3, pp. 229–246, Sep. 2012.
- [8] Y. Hou *et al.*, "The state-of-the-art review on applications of intrusive sensing, image processing techniques, and machine learning methods in pavement monitoring and analysis," *Engineering*, vol. 7, no. 6, pp. 845–856, Jun. 2021.
- [9] J. Fraden, *Handbook Modern Sensors*. New York, NY, USA: Springer, 2010.
- [10] M. Stocker, M. Ronkko, and M. Kolehmainen, "Situational knowledge representation for traffic observed by a pavement vibration sensor network," *IEEE Trans. Intell. Transp. Syst.*, vol. 15, no. 4, pp. 1441–1450, Aug. 2014.
- [11] M. Stocker, P. Silvonen, M. Rönkkö, and M. Kolehmainen, "Detection and classification of vehicles by measurement of road-pavement vibration and by means of supervised machine learning," *J. Intell. Transp. Syst.*, vol. 20, no. 2, pp. 125–137, 2016.
- [12] D. Kleyko, R. Hostettler, N. Lyamin, W. Birk, U. Wiklund, and E. Osipov, "Vehicle classification using road side sensors and feature-free data smashing approach," in *Proc. IEEE 19th Int. Conf. Intell. Transp. Syst. (ITSC)*, Nov. 2016, pp. 1988–1993.
- [13] Y. Huang, L. Wang, Y. Hou, W. Zhang, and Y. Zhang, "A prototype IoT based wireless sensor network for traffic information monitoring," *Int. J. Pavement Res. Technol.*, vol. 11, no. 2, pp. 146–152, Mar. 2018.
- [14] C. Zhang, S. Shen, H. Huang, and L. Wang, "Estimation of the vehicle speed using cross-correlation algorithms and MEMS wireless sensors," *Sensors*, vol. 21, no. 5, p. 1721, Mar. 2021.
- [15] W. Ma *et al.*, "A wireless accelerometer-based automatic vehicle classification prototype system," *IEEE Trans. Intell. Transp. Syst.*, vol. 15, no. 1, pp. 104–111, Feb. 2014.
- [16] R. Bajwa, R. Rajagopal, E. Coleri, P. Varaiya, and C. Flores, "In-pavement wireless weigh-in-motion," in *Proc. 12th Int. Conf. Inf. Process. Sensor Netw. (IPSN)*, 2013, pp. 103–114.
- [17] R. Bajwa, E. Coleri, R. Rajagopal, P. Varaiya, and C. Flores, "Pavement performance assessment using a cost-effective wireless accelerometer system," *Comput.-Aided Civil Infrastruct. Eng.*, vol. 35, no. 9, pp. 1009–1022, Sep. 2020.
- [18] Z. Ye *et al.*, "Real-time and efficient traffic information acquisition via pavement vibration IoT monitoring system," *Sensors*, vol. 21, no. 8, p. 2679, Apr. 2021.
- [19] Z. Ye, L. Wang, W. Xu, Z. Gao, and G. Yan, "Monitoring traffic information with a developed acceleration sensing node," *Sensors*, vol. 17, no. 12, p. 2817, Dec. 2017.
- [20] W. He, L. Deng, H. Shi, C. S. Cai, and Y. Yu, "Novel virtual simply supported beam method for detecting the speed and axles of moving vehicles on bridges," *J. Bridge Eng.*, vol. 22, no. 4, Apr. 2017, Art. no. 04016141.
- [21] L. Deng, W. He, Y. Yu, and C. S. Cai, "Equivalent shear force method for detecting the speed and axles of moving vehicles on bridges," *J. Bridge Eng.*, vol. 23, no. 8, Aug. 2018, Art. no. 04018057.
- [22] Z. Marszałek, T. Zeglen, R. Sroka, and J. Gajda, "Inductive loop axle detector based on resistance and reactance vehicle magnetic profiles," *Sensors*, vol. 18, no. 7, p. 2376, Jul. 2018.
- [23] E. O'Brien *et al.*, "Strategies for axle detection in bridge weigh-in-motion systems," in *Proc. Int. Conf. Weigh Motion (ICWIM)*, London, U.K.: Britain, 2012, pp. 79–88.
- [24] T. Bao, S. K. Babanajad, T. Taylor, and F. Ansari, "Generalized method and monitoring technique for shear-strain-based bridge weigh-in-motion," *J. Bridge Eng.*, vol. 21, no. 1, Jan. 2016, Art. no. 04015029.

- [25] M. Lydon, D. Robinson, S. E. Taylor, G. Amato, E. J. O. Brien, and N. Uddin, "Improved axle detection for bridge weigh-in-motion systems using fiber optic sensors," *J. Civil Struct. Health Monitor.*, vol. 7, no. 3, pp. 325–332, Jul. 2017.
- [26] J. Gajda *et al.*, "A vehicle classification based on inductive loop detectors," in *Proc. 18th IEEE Instrum. Meas. Technol. Conf. (IMTC)*, May 2001, pp. 460–464.
- [27] S. Hochreiter and J. Schmidhuber, "Long short-term memory," *Neural Comput.*, vol. 9, no. 8, pp. 1735–1780, 1997.
- [28] A. Graves, *Supervised Sequence Labelling With Recurrent Neural Networks*. Munich, Germany: Technical Univ. Munich, 2008.
- [29] K. Cho *et al.*, "Learning phrase representations using RNN encoder-decoder for statistical machine translation," 2014, *arXiv:1406.1078*.
- [30] Z. Ye, H. Xiong, and L. Wang, "Collecting comprehensive traffic information using pavement vibration monitoring data," *Comput.-Aided Civil Infrastruct. Eng.*, vol. 35, no. 2, pp. 134–149, Feb. 2020.



Zhoujing Ye (Member, IEEE) received the B.S. degree in safety engineering from the China University of Labor Relations in 2012 and the Ph.D. degree in civil engineering from the University of Science and Technology Beijing (USTB). In March 2019, he joined the Faculty of National Center for Materials Service Safety (NCMS), USTB. His current research interests mainly include intelligent transportation infrastructure and safety assessment.



Ya Wei received the B.S. degree in highway and urban road engineering from Chang'an University, Xi'an, China, in 1997, the M.S. degree in highway and railway engineering from Southeast University, Nanjing, China, in 2000, and the Ph.D. degree in civil engineering materials from the University of Michigan, Ann Arbor, MI, USA.

She joined as an Assistant Professor at Tsinghua University, Beijing, China, in 2010, where she is currently an Associate Professor. She has authored two books and more than 100 journal articles. Her research interests include developing ultra-high performance cement-based materials and intelligent materials for transportation infrastructure, multi-scale characterizing and simulating mechanical properties of cement-based materials, optimized design and serviceability enhancement of concrete pavements, and mechanical analysis and structural optimization of long-span steel bridge pavement systems.



Weidong Zhang received the B.S. degree in automation engineering and the Ph.D. degree in control science and engineering from the University of Science and Technology Beijing (USTB) in 1996 and 2004, respectively.

From 2004 to 2007, he was an Assistant Professor at USTB, where he became an Associate Professor in 2007 and a Full Professor in 2013. From 2010 to 2011, he was a Visiting Scholar at the College of Industrial and Systems Engineering, Georgia Institute of Technology (Georgia Tech), Atlanta, GA, USA. Since May 2021, he has been the Vice President of USTB. He has authored more than 50 journal articles. His research interests include intelligent control, system service reliability, and life prediction.



Linbing Wang received the B.S. degree in hydraulic engineering from Hohai University, Nanjing, China, in 1984, the M.S. degree in geotechnical engineering from Tongji University, Shanghai, China, in 1991, and the Ph.D. degree in civil engineering from the Georgia Institute of Technology (Georgia Tech), Atlanta, GA, USA, in 1998.

From 2000 to 2005, he was an Assistant Professor with Louisiana State University, Baton Rouge, LA, USA. In 2005, he joined as an Associate Professor at the Virginia Polytechnic Institute and State University (Virginia Tech), Blacksburg, VA, USA, where he became a Full Professor in 2010. He is also an Adjunct Professor with the University of Science and Technology Beijing. He has authored one book and more than 230 journal and proceeding articles. His research interests include smart and sustainable technologies, energy harvesting, health monitoring, innovative infrastructure assessment and performance predictions, high-performance materials, multiple-scale characterization, modeling and simulation, pavement testing and mechanistic pavement design, and infrastructure preservation and management.